Article:
Fairbairn, AI and Kelmanson, MA (2017) Spectrally accurate Nyström-solver error bounds for 1-D Fredholm integral equations of the second kind. Applied Mathematics and Computation, 315. pp. 211-233. ISSN 0096-3003

https://doi.org/10.1016/j.amc.2017.07.034

Spectrally accurate Nyström-solver error bounds for 1-D Fredholm integral equations of the second kind

Abigail I Fairbairn and Mark A Kelmanson*

Department of Applied Mathematics, University of Leeds, Leeds LS2 9JT, UK

Abstract

We present the theory underlying and computational implementation of analytical predictions of error bounds for the approximate solution of one-dimensional Fredholm integral equations of the second kind. Through asymptotic estimates of near-supremal operator norms, readily implementable formulae for the error bounds are computed explicitly using only the numerical solution of Nyström-based methods on distributions of nodes at the roots or extrema of diverse orthogonal polynomials. Despite the predicted bounds demanding no *a priori* information about the exact solution, they are validated to be spectrally accurate upon comparison with the explicit computational error accruing from the numerical solution of a variety of test problems, some chosen to be challenging to approximation methods, with known solutions. Potential limitations of the theory are discussed, but these are shown not to arise in the numerical computations.

Keywords: Fredholm integral equations, error bounds, spectral, collocation and related methods
2010 MSC: 45B05, 65L70, 65M70

1. Introduction

A large body of literature addresses the computation of approximate numerical solutions of one-dimensional Fredholm integral equations (FIEs) of the second kind, comprehensive overviews of which appear in [1, 2, 3, 4], each of which contains extensive theory and details of the implementation of diverse approximation techniques predominantly based on interpolation, projection, collocation and quadrature. Attestation to the widespread and continuing interest in the numerical solution of FIEs is reflected in the development and/or application of a diverse range of approximation techniques including (in chronological order of appearance) degenerate-kernel [5], multigrids [6], approximation theory [7], discrete product integration [8], Chebyshev polynomials [9, Chs.8-9], Adomian decomposition [10], Taylor series [11, 12], multi-FIE systems [13], Haar wavelets [14], fast matrix-vector algorithms [15] and piecewise-linear basis functions [16].

Despite the ongoing development of approximation methods for solving the diverse FIEs emerging in the modelling of applications in applied mathematics, engineering and fluid mechanics, practical tech-

*Corresponding author email address: M.Kelmanson@leeds.ac.uk

niques for determining computable, explicit, *a priori* error bounds, particularly for the spectrally accurate and widely used Nyström method, remain relatively scarce in the literature, attention notably focussing on only convergence rates (see, e.g., [17, §4.2.3]). The scarcity has elicited comment: in [2, p.158] it is asserted that *"these bounds will be difficult to evaluate in applications"*, and in [18] it is noted that, in the *"actual numerical computation [of error bounds]"*, there are *"only some scattered results that apply this approach"*. Examples of such results include those for degenerate-kernel FIEs [4, p.32] and for general FIEs [19, 20], upon the latter of which the present work builds with specific reference to spectrally accurate and ubiquitous Nyström methods.

In [20] it is shown how a theoretical error analysis can be implemented in such a way that the computed approximate solution of an FIE can be used to yield spectrally accurate *a priori* error predictions, in the absence of an exact solution, by using abscissae at the Legendre roots in order to optimise quadrature performance. However, for integro-differential equations (IDEs) augmented by end-point boundary conditions, the optimal asbcissae for differentiation are well-known to be the Chebyshev extrema, and hence an inefficient and costly interpolation between the optimal quadrature and optimal differentiation nodes is required. This cost is fully bypassed in the present paper, in which an error analysis based on near-optimal quadrature and differentiation using abscissae at both Radau nodes (one boundary condition) and Legendre extrema (two boundary conditions) is presented. The extension to the full analysis for IDEs is deferred to a companion paper.

The remainder of this paper is structured as follows. In §2.1 is presented an overview of relevant properties of quadrature formulae for each of the above-mentioned abscissae. In §2.2 is presented a brief overview of the well-known Nyström method in order to establish the framework for the error analysis in §2.3. In §2.4 an asymptotic analysis is undertaken of the conditions to be satisfied when estimating "near-suprema" functions to compute the required operator norms in the error formulae, since the true suprema are *a priori* unknown. In §3.1 are introduced a series of test problems, of distinct qualitative forms, the choice of which is motivated by consideration of examples that are well known to be challenging to approximation methods. The operator norms for these problems are computed in §3.2, in which it is shown that the criteria developed in §2.4 are met. In §3.3, error bounds are computed for the test problems and are shown to be in impressive agreement with the true computational errors, thereby validating the newly presented theory. By considering a more complex example than those considered in §3.3, the paper concludes in §4 with a discussion of the potential limitations of the approach, which transpire not to manifest themselves in practice.

2. Theory

2.1. Spectrally accurate numerical quadrature

The tools required to perform spectrally accurate numerical quadrature, implemented in §2.2, are first established. The canonical form, scaled into the interval $[-1, 1]$, of the linear Fredholm integral equation

of the second kind (FIE) for the unknown function $y(x)$ is

$$y(x) - \lambda \int_{-1}^{1} K(x,\xi)\, y(\xi)\, d\xi = g(x), \quad x \in [-1,1]\,, \tag{1}$$

in which the source function $g : [-1,1] \to \mathbb{R}$ and kernel $K : [-1,1] \times [-1,1] \to \mathbb{R}$ are prescribed functions, and $\lambda \in \mathbb{R}$ is a constant. In symbolic form, (1) is

$$y - \lambda \mathcal{K}\, y = g\,, \tag{2}$$

in which $y,\ g \in \mathcal{C} = C[-1,1]$, the Banach space, with supremum norm $\|\cdot\|$, on which $\mathcal{K}$ is a compact linear integral operator whose action on y is defined by

$$\mathcal{K}\, y = (\mathcal{K}\, y)(x) \equiv \int_{-1}^{1} K(x,\xi)\, y(\xi)\, d\xi\,. \tag{3}$$

It is assumed here, and throughout the rest of the paper, that λ is not a characteristic value of (1), which therefore [2] has the unique solution $y(x)$.

In the Nyström method, the action of $\mathcal{K}$ on y is approximated by $\mathcal{K}_N$, the finite-rank quadrature operator on $\mathcal{C}$ defined as the discrete counterpart of (3),

$$\mathcal{K}_N\, y = (\mathcal{K}_N\, y)(x) \equiv \mathbf{k}_N(x)^T \mathbf{y}\,, \tag{4}$$

in which

$$\{\mathbf{k}_N(x)\}_j = w_{j,N} K(x, \xi_{j,N}) \quad \text{and} \quad \{\mathbf{y}\}_j = y(\xi_{j,N})\,, \quad j = 1, \ldots, N\,, \tag{5}$$

wherein $w_{j,N}$ and $\xi_{j,N}$ are respectively the weights and abscissae of the rule, which is Gaussian since the integral in (3) has unit weight function. Mindful of concurrent related work on integro-differential FIEs (IDEs) with unit weight function, the present work develops error bounds based on not only the more commonly encountered Gauss-Legendre (hereafter Legendre) quadrature but also, because of the end-point boundary conditions augmenting the IDEs, on formulae with assigned abscissae at $x = \pm 1$ such as Legendre Gauss-Radau (hereafter Radau) quadrature and Legendre-Gauss-Lobatto (hereafter Lobatto) quadrature.

Relevant standard results (see, e.g., [21, Ch.8]) for the different quadrature formulae are now collected for convenience. To simplify subsequent presentation, define the quadrature error $\mathcal{Q}_N$ for $x \in [-1,1]$ by

$$\mathcal{Q}_N \equiv \|\mathcal{K}\, y - \mathcal{K}_N\, y\|\,, \tag{6}$$

in which here and subsequently the supremum norm of the Banach space $\mathcal{C} = C[-1,1]$ is implied. Also define the auxiliary value $\mathbb{K}_M$ by

$$\mathbb{K}_M \equiv \max_{x,\xi \in [-1,1]} \left| \frac{\partial^M}{\partial \xi^M} \big(K(x,\xi)\, y(\xi) \big) \right|\,, \tag{7}$$

which is recognised as the supremum norm of the factor occurring in the remainder of mean-value-theorem error term: it merits attention that this will overestimate the error because the correct $\xi \in [-1,1]$ cannot be determined *a priori*.

In Table 1 is presented a summary of the results (some standard, some presently derived) needed for implementing the theoretical error analysis in §2.3 for the three quadrature methods listed above. If the convention is henceforth adopted that bracketed superscripts denote the number of assigned abscissae in the rule, the last two rows of Table 1 reveal that the asymptotic bound $\widetilde{\beta}_N^{(\nu)}$ as $N \to \infty$ on all three quadrature errors $\mathcal{Q}_N$ is given by the single formula

$$\mathcal{Q}_N \equiv \|(\mathcal{K} - \mathcal{K}_N)\, y\| \leq \widetilde{\beta}_N^{(\nu)} \sim \frac{\pi\ N^\nu\, \mathbb{K}_{2N-\nu}}{4^{N-\nu}(2N)!}\,, \quad \nu = 0,\ 1,\ 2\,, \tag{8}$$

in which $\nu = 0,\ 1$ and 2 correspond respectively to Legendre, Radau and Lobatto quadrature, and in which the coefficient of $\mathbb{K}_{2N-\nu}$ is exact for $\nu = 1$ and in error by less than 10^{-10} for $N \geq 6$ when $\nu = 0, 2$.

The predicted bound (8) is validated on a test example, fully summarised in Figure 1, which demonstrates the spectral convergence to zero of $\mathcal{Q}_N$ on all three nodal distributions. For completeness, in Figure 2 are presented complex equipotentials of the monic polynomials associated with the nodal distributions; the sub-figure relating to Lobatto nodes is presented in [22, p.130], but those relating to the Legendre, left- and right-Radau nodes have not, to the authors' knowledge, appeared elsewhere.

2.2. Nyström method

The approximate solution $y_N(x)$ of (1) is given by the Nyström method as the solution of

$$y_N(x) - \lambda\, \mathbf{k}_N(x)^T \mathbf{y}_N = g(x), \quad x \in [-1, 1]\,, \tag{9}$$

in which $\mathbf{k}_N(x)$ is defined in (5) and $\{\mathbf{y}_N\}_j = y_N(\xi_{j,N})$ for $j = 1, \ldots, N$. The symbolic form of (9) is (*cf.* (2))

$$y_N - \lambda\, \mathcal{K}_N\, y_N = g\,. \tag{10}$$

Collocating (9) at the N nodes $x = \xi_{i,N},\ i = 1, \ldots, N$, yields an $N \times N$ linear system for the vector $\mathbf{y}_N$ of nodal values $y_N(\xi_{j,N}),\ j = 1, \ldots, N$, namely

$$(\mathbf{I} - \lambda\, \mathbf{K}_N)\, \mathbf{y}_N = \mathbf{g}_N\,, \tag{11}$$

wherein the elements, for $i, j = 1, \ldots, N$, are given by the explicit formulae

$$\{\mathbf{y}_N\}_i = y_N(\xi_{i,N})\,, \quad \{\mathbf{g}_N\}_i = g(\xi_{i,N})\,, \quad \{\mathbf{K}_N\}_{i,j} = w_{j,N} K(\xi_{i,N}, \xi_{j,N})\,.$$

Solution of the system (11) provides the vector $\mathbf{y}_N$ in the Nyström inversion formula (*cf.* (9))

$$y_N(x) = g(x) + \lambda\, \mathbf{k}_N(x)^T \mathbf{y}_N\,, \quad x \in [-1, 1]\,, \tag{12}$$

for the approximation $y_N(x)$ of $y(x)$ which, via (7) and (8), will agree to machine precision if the product $K(x, \xi)\, u(\xi)$ in (1) is a polynomial in ξ of degree less than or equal to $2N - 1 - \nu$.

2.3. Error analysis framework

Subtracting (10) from (2) yields the error

$$y - y_{_N} = \lambda\,(\mathcal{K}\,y - \mathcal{K}_{_N}\,y_{_N}) = \lambda\,\mathcal{K}\,(y - y_{_N}) + \lambda\,(\mathcal{K} - \mathcal{K}_{_N})\,y_{_N}\,,$$

hence the error can be expressed in terms of (only) the approximate solution $y_{_N}$ as

$$y - y_{_N} = \lambda\,(\mathcal{I} - \lambda\,\mathcal{K})^{-1}(\mathcal{K} - \mathcal{K}_{_N})\,y_{_N}\,, \tag{13}$$

in which $\mathcal{I}$ is the identity operator and the existence and boundedness of $(\mathcal{I} - \lambda\,\mathcal{K})^{-1}$ is guaranteed [2, Thm. 3.4] by y being the unique solution of (2), equivalently $(\mathcal{I} - \lambda\,\mathcal{K})\,y = g$. It is well known that standard error analyses, based upon the convergence with N of $\|\mathcal{K} - \mathcal{K}_{_N}\|$, cannot be similarly conducted for the Nyström method, since the pointwise convergence $\|\mathcal{K}\,y_{_N} - \mathcal{K}_{_N}\,y_{_N}\| \to 0$ as $N \to \infty$ is not reflected in norm convergence; specifically (see, e.g., [2, Thm. 12.8][1]),

$$\|\mathcal{K} - \mathcal{K}_{_N}\| \geq \|\mathcal{K}\|\,, \quad N \to \infty\,,$$

so that one must utilise the auxiliary results [4, (4.1.19)]

$$\|(\mathcal{K} - \mathcal{K}_{_N})\,\mathcal{K}\,\| \to 0\,, \quad \|(\mathcal{K} - \mathcal{K}_{_N})\,\mathcal{K}_{_N}\,\| \to 0\,, \quad N \to \infty\,,$$

using which a bound $\mathcal{F}_{_N}$ on the inverse operator in (13) can be determined as in, e.g., [3, (4.7.17b)]). Since the quadrature scheme (4) is (by (6), (7) and the information in the last row of Table 1) convergent for all continuous functions on $\mathcal{C}$ then, for sufficiently large N, $(\mathcal{I} - \lambda\,\mathcal{K}_{_N})^{-1}$ exists and is uniformly bounded [4, Thm. 4.1.2], and

$$\left\|(\mathcal{I} - \lambda\,\mathcal{K})^{-1}\right\| \leq \mathcal{F}_{_N} \equiv \frac{1 + |\lambda|\;\left\|(\mathcal{I} - \lambda\,\mathcal{K}_{_N})^{-1}\right\|\;\|\mathcal{K}\|}{1 - \lambda^2\;\left\|(\mathcal{I} - \lambda\,\mathcal{K}_{_N})^{-1}\right\|\;\|(\mathcal{K} - \mathcal{K}_{_N})\,\mathcal{K}\|}\,, \tag{14}$$

which defines the factor $\mathcal{F}_{_N}$ and in which the denominator is by construction positive [23]. Then (13) yields a bound on the error norm $\mathcal{E}_{_N}$ given by

$$\mathcal{E}_{_N} \equiv \|y - y_{_N}\| \leq \mathcal{F}_{_N}\;\|\lambda\,(\mathcal{K} - \mathcal{K}_{_N})\,y_{_N}\|\,, \tag{15}$$

from which (10) yields the Nyström error bound in the form [20, (10.20)]

$$\mathcal{E}_{_N} \leq \mathcal{B}_{_N} \equiv \mathcal{F}_{_N}\;\|y_{_N} - \lambda\,\mathcal{K}\,y_{_N} - g\|\,, \tag{16}$$

which both defines the bound $\mathcal{B}_{_N}$ and expresses the approximation error in terms of only the numerical solution $y_{_N}$ and has the advantage that it can be used to compute the error explicitly without the need for the intermediate calculation of $\mathcal{K}_{_N}\,y_{_N}$.

[1] Consider, e.g., $y_{_N}(x)$ to be unity everywhere except for N inverted "spikes" of unit height and infinitesimal width at the quadrature abscissae, so that $y_{_N}(\xi_{j,_N}) = 0,\ j = 1, \ldots, N$ and hence $\|\mathcal{K}_{_N}\| = 0$.

2.4. Asymptotic error analysis

Attention now turns to the computation of the three sub-bounds in $\mathcal{F}_{_N}$ defined in (14). Although $\mathcal{F}_{_N}$ is established (albeit in a different form) in [3, 4], is not developed therein into a computable quantity (see motivating remarks from [2, 18] in §1). Rewrite (14) in supremum form,

$$\mathcal{F}_{_N} = \frac{1 + |\lambda| \sup\limits_{u\in\mathcal{C}} \dfrac{\big\|(\mathcal{I} - \lambda\,\mathcal{K}_{_N})^{-1} u\big\|}{\|u\|} \sup\limits_{v\in\mathcal{C}} \dfrac{\|\mathcal{K}\,v\|}{\|v\|}}{1 - \lambda^2 \sup\limits_{u\in\mathcal{C}} \dfrac{\big\|(\mathcal{I} - \lambda\,\mathcal{K}_{_N})^{-1} u\big\|}{\|u\|} \sup\limits_{w\in\mathcal{C}} \dfrac{\|(\mathcal{K} - \mathcal{K}_{_N})\,\mathcal{K}\,w\|}{\|w\|}}\,, \tag{17}$$

and let the *a priori* unknown functions $\widetilde{u},\ \widetilde{v},\ \widetilde{w} \in \mathcal{C}$ yield the required suprema in (17), so that

$$\mathcal{F}_{_N} = \frac{(\|\widetilde{u}\|\ \|\widetilde{v}\| + |\lambda|\ \big\|(\mathcal{I} - \lambda\,\mathcal{K}_{_N})^{-1}\widetilde{u}\big\|\ \|\mathcal{K}\,\widetilde{v}\|)\ \|\widetilde{w}\|}{(\|\widetilde{u}\|\ \|\widetilde{w}\| - \lambda^2\ \|(\mathcal{I} - \lambda\,\mathcal{K}_{_N})^{-1}\widetilde{u}\|\ \|(\mathcal{K} - \mathcal{K}_{_N})\,\mathcal{K}\,\widetilde{w}\|)\ \|\widetilde{v}\|}\,. \tag{18}$$

It is clear that further progress on the development of a computable bound demands estimation of the unknown $\widetilde{u},\ \widetilde{v},\ \widetilde{w} \in \mathcal{C}$ on the assumption that near-suprema functions, $u,\ v,\ w \in \mathcal{C}$ respectively, can be chosen. Moreover, Table 1 reveals that the term $\|(\mathcal{K} - \mathcal{K}_{_N})\,\mathcal{K}\,\widetilde{w}\|$ in the denominator of $\mathcal{F}_{_N}$ will decay exponentially[2] with N because of its error factor $\psi_{_N}^{(\nu)}$ associated with the action of the operator $\mathcal{K} - \mathcal{K}_{_N}$. Computation of $\mathcal{F}_{_N}$ therefore admits two levels of approximation.

An asymptotic analysis can be conducted by first defining a small positive parameter $0 < \epsilon \ll 1$ and $\mathcal{O}(1)$ constants $\alpha,\ \beta,\ \gamma \in \mathbb{R}$ such that

$$\big\|(\mathcal{I} - \lambda\,\mathcal{K}_{_N})^{-1}\big\| \equiv \frac{\big\|(\mathcal{I} - \lambda\,\mathcal{K}_{_N})^{-1}\widetilde{u}\big\|}{\|\widetilde{u}\|} = \frac{\big\|(\mathcal{I} - \lambda\,\mathcal{K}_{_N})^{-1} u\big\|}{\|u\|} + \alpha\,\epsilon\,, \quad \|\mathcal{K}\| \equiv \frac{\|\mathcal{K}\,\widetilde{v}\|}{\|\widetilde{v}\|} = \frac{\|\mathcal{K}\,v\|}{\|v\|} + \beta\,\epsilon \tag{19}$$

and

$$\|(\mathcal{K} - \mathcal{K}_{_N})\,\mathcal{K}\| \equiv \frac{\|(\mathcal{K} - \mathcal{K}_{_N})\,\mathcal{K}\,\widetilde{w}\|}{\|\widetilde{w}\|} = \frac{\|(\mathcal{K} - \mathcal{K}_{_N})\,\mathcal{K}\,w\|}{\|w\|} + \gamma\,\epsilon\,. \tag{20}$$

For sufficiently large N, (8) reveals that

$$\|(\mathcal{K} - \mathcal{K}_{_N})\,\mathcal{K}\,w\| \sim \mathcal{W}_{_N}^{(\nu)} \equiv \frac{\pi\ N^{\nu}\,\mathbb{M}_{2N-\nu}}{4^{N-\nu}(2N)!}\,, \quad \nu = 0,\ 1,\ 2\,, \tag{21}$$

in which, by extension of (7), the constant $\mathbb{M}_{2N-\nu}$ is found using

$$\mathbb{M}_{_M} \equiv \max_{x,\xi\in[-1,1]} |\mathcal{M}_{_M}(x,\xi)| \quad \text{where} \quad \mathcal{M}_{_M}(x,\xi) \equiv \frac{\partial^{_M}}{\partial\xi^{_M}} \left(K(x,\xi) \int_{-1}^{1} K(\xi,\eta)\,w(\eta)\,d\eta \right). \tag{22}$$

Thus for sufficiently large N, say $N \geq N_{\epsilon}$, (21), (22) and Stirling's formula reveal that, in (20),

$$\|(\mathcal{K} - \mathcal{K}_{_N})\,\mathcal{K}\| = \mathcal{O}(\epsilon) \quad \text{provided} \quad \mathcal{W}_{_N}^{(\nu)} = o(\epsilon)\,, \tag{23}$$

which is true for all $\epsilon > 0$ provided that the growth-rate of $\mathbb{M}_{2N-\nu}$ is less than $\mathcal{O}\big(N^{\alpha\,N}\big)$. Large-$N$ asymptotics applied to $\mathcal{W}_{_N}^{(\nu)}$ defined in (21) reveal that condition (23) is met providing

$$\alpha < 2 + (4\ln 2 - 2)\big((\ln N)^{-1} - (\ln N)^{-2}\big) + o\big((\ln N)^{-2}\big)\,, \quad N \to \infty\,. \tag{24}$$

[2]This assertion is demonstrated to be true in §3.3.

Hence, if $\mathbb{M}_{2N-\nu} \leq \mathcal{O}\big(N^{2N}\big)$, condition (23) is satisfied and (18)–(23) yield

$$\mathcal{F}_{N} = 1 + \frac{|\lambda| \, \big\|(\mathcal{I} - \lambda\,\mathcal{K}_{N})^{-1} u\big\| \, \|\mathcal{K}\, v\|}{\|u\| \, \|v\|} + \mathcal{O}(\epsilon)\,, \quad N \geq N_{\epsilon}\,. \tag{25}$$

The event that the condition $\mathbb{M}_{2N-\nu} \leq \mathcal{O}\big(N^{2N}\big)$ is potentially not met requires a more detailed analysis; for clarity this is considered separately in §4.

The practical choice of norm-maximisation functions $u,\ v \in \mathcal{C}$ in the leading-order term on the right-hand side of (25) is addressed in §3; these shall henceforth be termed "trial" functions. With u chosen, let $U_{N} \in \mathcal{C}$ be the solution of (*cf.* (10))

$$U_{N} - \lambda\,\mathcal{K}_{N}\,U_{N} = u\,. \tag{26}$$

The function U_{N} can be computed cheaply in parallel with y_{N} because the discretised form of (26) can be solved simultaneously with (11) to give, in an obvious notation, the $N \times N$ partitioned linear system

$$(\mathbf{I} - \lambda\,\mathbf{K}_{N})\,(\mathbf{y}_{N} \big| \mathbf{U}_{N}) = (\mathbf{g}_{N} \big| \mathbf{u}_{N})\,, \tag{27}$$

for the nodal values of both y_{N} and U_{N}. An adapted form of (12) now yields the inversion formula

$$U_{N}(x) = u(x) + \lambda\,\mathbf{k}_{N}(x)^{T}\mathbf{U}_{N}\,, \quad x \in [-1, 1]\,. \tag{28}$$

With u and v chosen, the computable leading-order bound $\mathcal{F}_{N}$ on the inverse in (14) is finally derived using (25) and (26) as

$$\mathcal{F}_{N} = 1 + \frac{|\lambda| \, \|U_{N}\| \, \|\mathcal{K}\, v\|}{\|u\| \, \|v\|} \tag{29}$$

which, together with (16), allows computation of the required bound $\mathcal{B}_{N}$ on the Nyström error $\mathcal{E}_{N}$.

3. Implementation, results and discussion

3.1. Motivation of test problems

The theory of §2 is now implemented on four test problems with known solutions of qualitatively different form. For each problem, the source function $g(x)$ is readily generated directly from (1) from the known solution $y(x)$, parameter λ and kernel $K(x, \xi)$, and hence their (cumbersome) forms are not reproduced here.

3.2. Computation of operator norms

The need to compute the norm $\|\mathcal{K}\, v\|$ in (29) arises through the manipulation of (14), which defines $\mathcal{F}_{N}$ in terms of both $\|\mathcal{K}\|$ and $\|(\mathcal{K} - \mathcal{K}_{N})\,\mathcal{K}\|$. It is worthy of note that the former norm has previously been defined [4, (1.2.21)] as

$$\|\mathcal{K}\,\| \equiv \max_{x \in [-1,1]} \int_{-1}^{1} |K(x, \xi)|\, d\xi \tag{30}$$

which differs from the standard form

$$\|\mathcal{K}\| \approx \frac{\|\mathcal{K}\,1\|}{\|1\|} = \max_{x\in[-1,1]} \left| \int_{-1}^{1} K(x,\xi)\, d\xi \right| . \tag{31}$$

That is, (30) implicitly assumes the choice of trial function $v \equiv 1$ in (29); it also portends evaluation of a looser bound than (31) because of the modulus signs on the integrand instead of the integral. For completeness, it is recorded that, in deriving $\|(\mathcal{K} - \mathcal{K}_N)\,\mathcal{K}\|$ in [4, (4.1.13)–(4.1.17)], $w \equiv 1$ has similarly been chosen in [4, (4.1.14)].

In all results pertaining to the test problems, computations have been performed using the "external" form

$$\|\mathcal{K}\,v\| = \max_{x\in[-1,1]} \left| \int_{-1}^{1} K(x,\xi)\, v(\xi)\, d\xi \right| , \tag{32}$$

whose alternative "internal" form suggested by (30) is

$$\|\mathcal{K}\,v\| = \max_{x\in[-1,1]} \int_{-1}^{1} |K(x,\xi)\, v(\xi)|\, d\xi\,. \tag{33}$$

The ratio $\|\mathcal{K}\,v\| \,/\, \|v\|$ appearing in $\mathcal{F}_N$ is computed using (32) and (33) and compared in Table 3, in which can be seen that the choice of trial function has a marked effect on the magnitude of $\|\mathcal{K}\,v\| \,/\, \|v\|$ (upon which the error estimate depends linearly). Guided by (31), $v = 1$ is chosen as one trial function; two other natural candidates are $v = g$ and $v = y$. As expected, and as seen in Table 3, the external formula gives the tighter bound; in those cases where there are end-point maxima, the internal and external computations yield identical results. Moreover, $\|\mathcal{K}\,v\| \,/\, \|v\|$ is in all cases maximised when using the trial function $v = 1$, i.e. when $\|\mathcal{K}\|$ is computed using (31): this supports the use of (30) (i.e. [4, (1.2.21)], which is presented without discussion) which, for the reasons outlined above, would give looser error bounds than (31). Therefore, the trial function $v = 1$ is used hereafter to estimate $\|\mathcal{K}\|$ as the supremum of $\|\mathcal{K}\,v\| \,/\, \|v\|$.

3.3. Results for test problems

With $v = 1$ chosen, the remaining required norm in (29) is $\|U_N\| \,/\, \|u\|$, i.e. $\left\|(\mathcal{I} - \lambda\,\mathcal{K}_N)^{-1}u\right\| \,/\, \|u\|$, in which U_N is determined numerically via (26) upon specification of the trial function u. However, since in the numerical experiments the exact solution y is deemed to be unknown, the (available) numerical solution $u = y_N$ computed using (12) is now chosen as one of the trial functions on the basis of the expected convergence of y_N to y with increasing N. The two trial functions $u = 1$ and $u = g$ tested in Table 3 are also used. Computed values of $\|U_N\| \,/\, \|u\|$, now dependent upon N, are presented in Table 4. Now evident is that, for a given u, the values of $\|U_N\| \,/\, \|u\|$ all converge with N, and again evident is that the maximal values occur for $u = 1$. Hence the trial function $u = 1$ is used hereafter to estimate $\left\|(\mathcal{I} - \lambda\,\mathcal{K}_N)^{-1}\right\|$ as the supremum of $\left\|(\mathcal{I} - \lambda\,\mathcal{K}_N)^{-1}u\right\| \,/\, \|u\|$.

For clarity, the error-estimation procedure so far developed is now summarised: (a) trial functions $u = 1$ and $v = 1$ are chosen; (b) $\|\mathcal{K}\,v\| \,/\, \|v\|$ is computed using (32); (c) U_N is computed using (26)–(28); (d) $\mathcal{F}_N$ is computed using (29); (e) the required error bound $\mathcal{B}_N$ is computed using (16) and compared with

the true numerical error $\mathcal{E}_N$ computed using (15). Before this comparison is made, it remains only to check that condition (23) is satisfied, without which the estimate of $\mathcal{F}_N$ in (29) is not justified.

Via (21), (22) and Table 2, $\mathcal{W}_N^{(\nu)}$ is, independently of ν and trial function w, identically zero for Problems 1, 2 and 3 when $N > 3$. For Problem 4, $\mathcal{W}_N^{(\nu)}$ exhibits spectral convergence with N irrespective of ν, and hence there exists an N_ϵ such that (23) is satisfied. Figure 3 depicts this spectral convergence for $\nu = 0$ and $w = 1$, $w = g$ and $w = y_N$; results for $\nu = 1, 2$ exhibit qualitatively identical behaviour.

A preliminary comparison of $\mathcal{B}_N$ and $\mathcal{E}_N$ is effected in Table 5, which summarises the results of the numerical experiments. It is evident that the ratio $\mathcal{B}_N/\mathcal{E}_N$ for $u = v = 1$: converges with increasing N; exceeds unity throughout, and; is always strictly of order $\mathcal{O}(1)$. Hence for the four test problems, three of which are challenging to approximation methods, the present theory yields tight predictions of error bounds, extremely so for Problem 4. A different approach used by the authors in [20, (10.24)] implicitly fixes the choice $u = g$, in which case $U_N = y_N$ via (27) and $v = y_N$, although this may yield (for the reasons evident in Table 3) "bounds" satisfying $\mathcal{B}_N/\mathcal{E}_N < 1$.

A full comparison of predicted bounds and actual computational errors is presented in Figure 4, in which attention is drawn to the disparate vertical scales in the sub-plots. As expected, the error convergence rate for the "smooth" problem is by far the most rapid, so that the largest relative factors in Table 5 are in a sense mitigated by acting upon the smallest values of $\|y_N - \lambda\,\mathcal{K}\,y_N - g\|$ in (16), as quantified in Table 6. The "Runge" problem has the largest error magnitudes because of the behaviour of the higher derivatives of the solution implicit in (7); even so, the error-to-bound relative ratios are no worse than for the "smooth" problem, as Table 5 confirms. The error magnitudes in the "steep" and "highly oscillatory" problems are similar, although the latter is noticeably larger for smaller values of N; this is an expected feature of the inability to resolve the oscillations in y_N for the low-N spatial discretisations; for both problems, the error bounds are accurately predicted for sufficiently large N.

4. Potential limitations of the error analysis

The caveat raised immediately after (25) is now addressed. When the denominator of $\mathcal{F}_N$ defined in (14) is negative, the conditions of the theorem [4, Thm. 4.1.2] that underlies (14) are not met. This may possibly occur if, via (23), $\|(\mathcal{K} - \mathcal{K}_N)\,\mathcal{K}\|$ grows at a rate faster than N^{2N}. Since (see caption of Figure 3) the meeting of condition (23) is effectively dependent upon only $K(x,\xi)$ and the quadrature nodes, it is sufficient to consider a potentially problematic "Runge" kernel, an example of which is

$$K(x,\xi) = \frac{\xi - x}{1 + \alpha^2\,\xi^2}\,, \quad x, \xi \in [-1, 1]\,, \tag{34}$$

and for which (22) gives

$$\mathcal{M}_0(x,\xi) = \frac{2\,(x-\xi)\,\xi\,\tan^{-1}\alpha}{\alpha\,(1 + \alpha^2\,\xi^2)}\,, \tag{35}$$

whose successive partial derivatives with respect to ξ grow exponentially for sufficiently large α. It is possible to show that the suprema of $\mathcal{M}_M(x,\xi)$ are at $x = \pm 1$ for all M, and that the $\mathcal{M}_M(x,\xi)$ can be

normalised to $\mu_{\scriptscriptstyle M}(x,\xi)$ using the scaling

$$\mu_{\scriptscriptstyle M}(x,\xi) = \frac{\alpha^{2-M}}{2M!\,\tan^{-1}\alpha}\,\mathcal{M}_{\scriptscriptstyle M}(x,\xi)\,, \quad \|\mu_{\scriptscriptstyle M}\| \le 1\,, \quad M \in \mathbb{N}\,. \tag{36}$$

Via (21), (22) and (36) it follows that

$$\mathcal{W}_{\scriptscriptstyle N}^{(0)} = \frac{\pi}{2}\left(\frac{\alpha}{2}\right)^{2N-2}\tan^{-1}\alpha\,, \quad \mathcal{W}_{\scriptscriptstyle N}^{(1)} = \frac{2}{\alpha}\,\mathcal{W}_{\scriptscriptstyle N}^{(0)} \quad \text{and} \quad \mathcal{W}_{\scriptscriptstyle N}^{(2)} = \frac{4N}{(2N-1)\alpha}\,\mathcal{W}_{\scriptscriptstyle N}^{(1)}\,, \tag{37}$$

and hence the maximal estimate $\mathcal{W}_{\scriptscriptstyle N}^{(\nu)}$ of $\|(\mathcal{K}-\mathcal{K}_{\scriptscriptstyle N})\,\mathcal{K}\,\|$ portends a breakdown of the theory when $\alpha > 2$ on all node distributions considered. However, this transpires not to be the case in practice when, as Figure 5 reveals, $\|(\mathcal{K}-\mathcal{K}_{\scriptscriptstyle N})\,\mathcal{K}\,\|$ (computed using $w = 1$) converges to zero spectrally with increasing N and α despite (37) predicting exponential divergence when $\alpha > 2$. Clearly evident in Figure 5 is not only this spectral convergence with N to zero of the numerically computed $\|(\mathcal{K}-\mathcal{K}_{\scriptscriptstyle N})\,\mathcal{K}\,\|$, but also the unexpected independence upon α for $\alpha \gg 1$. That is, in practice, the theory presented in §2 holds for even the ostensibly problematic-by-construction "Runge" kernel (34).

In order to explain the apparent convergence-divergence discrepancy portrayed in Figure 5, it is necessary to examine not the bound $\mathbb{M}_{\scriptscriptstyle M}$ in (22), but rather the (normalised) function $\mu_{\scriptscriptstyle M}(x,\xi)$ in (36) upon which the bound is based. Figure 6 depicts $|\mu_6(x,\xi)|$ (alongside its logarithm) in order to show that its suprema are highly localised; specifically, it is straightforward to show that the leading-order large-α asymptotic behaviour of the mean of $\mu_{\scriptscriptstyle M}(x,\xi)$ is $\overline{\mu}_{\scriptscriptstyle M} \sim \big((-1)^{M+1}-1\big)/(2\,\alpha^{M+3})$, which confirms that the norm-to-mean discrepancy of $\mu_{\scriptscriptstyle M}$ increases exponentially with M and algebraically with $|\alpha|$ (see Figure 7). Hence, although the bound $\mathbb{M}_{\scriptscriptstyle M}$ is used in the error estimate, the true error term associated with Nyström integration requires the evaluation of $\mu_{\scriptscriptstyle M}(x,\xi)$ at an *a priori* unknown location (x^*,ξ^*), say. As can be seen from Figure 6, it will be the case (following denormalisation) that $|\mathcal{M}_{\scriptscriptstyle M}(x^*,\xi^*)| \ll \mathbb{M}_{\scriptscriptstyle M}$, thereby explaining the observation $\|(\mathcal{K}-\mathcal{K}_{\scriptscriptstyle N})\,\mathcal{K}\,\| \ll \mathcal{W}_{\scriptscriptstyle N}^{(0)}$ evident in Figure 5. Finally, Figure 7 evidences the increasing localisation, alluded to above, of the suprema of $|\mu_{\scriptscriptstyle M}(x,\xi)|$ with increasing $|\alpha|$.

In summary, the theoretical method proposed herein, and its computational implementation, has been fully validated via the results presented on a qualitatively diverse set of test problems. Its potential limitations have been discussed and demonstrated not to be realised in practice. The authors have recently extended the proposed method to the case of first-order Fredholm integro-differential equations of the second kind. The extended analysis, incorporating a detailed investigation of discrete spectral differentiation on orthogonal-polynomial node sets, is the subject of a forthcoming companion paper.

References

[1] C. Baker, The Numerical Treatment of Integral Equations, Clarendon Press, Oxford, 1977.

[2] R. Kress, Linear Integral Equations, Springer-Verlag, Berlin, 1989.

[3] W. Hackbusch, Integral Equations: Theory and Numerical Treatment, Birkhäuser Verlag, Basel, Switzerland, 1995.

[4] K. Atkinson, The Numerical Solution of Integral Equations of the Second Kind, Cambridge University Press, New York, 1997.

[5] I. H. Sloan, B. J. Burn, N. Datyner, A new approach to the numerical solution of integral equations, Journal of Computational Physics 18 (1975) 92–105.

[6] P. Hemker, H. Schippers, Multiple grid methods for the solution of Fredholm integral equations of the second kind, Mathematics of Computation 36 (1981) 215–232.

[7] L. Brutman, An application of the generalized alternating polynomials to the numerical solution of Fredholm integral equations, Numerical Algorithms 5 (1993) 437–442.

[8] H. Kaneko, Y. Xu, Gauss-type quadratures for weakly singular integrals and their application to Fredholm integral equations of the second kind, Mathematics of Computation 62 (1994) 739–753.

[9] J. C. Mason, D. Handscomb, Chebyshev Polynomials, CRC Press, Florida, 2002.

[10] E. Babolian, J. Biazar, A. Vahidi, The decomposition method applied to systems of Fredholm integral equations of the second kind, Appl. Math. Comput. 148 (2004) 443–452.

[11] K. Maleknejad, N. Aghazadeh, M. Rabbani, Numerical solution of second kind Fredholm integral equations system by using a Taylor-series expansion method, Applied Mathematics and Computation 175 (2006) 1229–1234.

[12] P. Huabsomboon, B. Novaprateep, H. Kaneko, On Taylor-series expansion methods for the second kind integral equations, Journal of Computational and Applied Mathematics 234 (2010) 1466–1472.

[13] M. De Bonis, C. Laurita, Numerical treatment of second kind Fredholm integral equations systems on bounded intervals, Journal of Computational and Applied Mathematics 217 (2008) 64–87.

[14] E. Babolian, A. Shahsavaran, Numerical solution of nonlinear Fredholm integral equations of the second kind using Haar wavelets, Journal of Computational and Applied Mathematics 225 (2009) 87–95.

[15] W.-J. Xie, F.-R. Lin, A fast numerical solution method for two dimensional Fredholm integral equations of the second kind, Appl. Numer. Math. 59 (2009) 1709–1719.

[16] E. Babolian, M. Mordad, A numerical method for solving systems of linear and nonlinear integral equations of the second kind by hat basis functions, Computers and Mathematics with Applications 62 (2011) 187–198.

[17] L. Delves, J. Mohamed, Computational Methods for Integral Equations, Cambridge, 1985.

[18] P. Linz, Bounds and estimates for condition numbers of integral equations, SIAM J. Numer. Anal. 28 (1991) 227–235.

[19] M. Kelmanson, M. C. Tenwick, Error reduction in Gauss-Jacobi-Nyström quadrature for Fredholm integral equations of the second kind, CMES 55 (2010) 191–210.

[20] A. Fairbairn, M. Kelmanson, Computable theoretical error bounds for Nyström methods for Fredholm integral equations of the second kind, in: P. Harris (Ed.), Proc. 10th UK Conf. on Boundary Integral Methods (Brighton, UK), 2015, pp. 85–94.

[21] F. B. Hildebrand, Introduction to Numerical Analysis, McGraw-Hill, New York, 1974.

[22] L. N. Trefethen, Approximation Theory and Approximation Practice, SIAM, Philadelphia, 2013.

[23] H. Brakhage, Über die numerische Behandlung von Integralgleichungen nach der Quadraturformelmethode, Numer. Math. 2 (1960) 183–196.

[24] J. P. Boyd, Defeating the Runge Phenomenon for equispaced polynomial interpolation via Tikhonov regularization, Applied Mathematics Letters 5 (1992) 57–59.

[25] J. P. Boyd, Exponentially accurate Runge-free approximation of non-periodic functions from samples on an evenly spaced grid, Applied Mathematics Letters 20 (2007) 971–975.

[26] L. N. Trefethen, Spectral Methods in MATLAB, SIAM, Philadelphia, 2000.

Quadrature	Legendre	Radau	Lobatto
Assigned $\xi_{j,N}$	None	$\xi_{1,N} = -1$	$\xi_{1,N} = -1,\ \xi_{N,N} = 1$
Weights	—	$w_{1,N} = \frac{2}{N^2}$	$w_{1,N} = w_{N,N} = \frac{2}{N(N-1)}$
Free $\xi_{j,N}$	$P_N(\xi_{j,N}) = 0$	$\frac{P_{N-1}(\xi_{j,N}) + P_N(\xi_{j,N})}{1+\xi_{j,N}} = 0$	$\frac{P'_{N-1}(\xi_{j,N})}{1-\xi_{j,N}^2} = 0$
Weights $w_{j,N}$	$\frac{-2}{(N+1)\,P'_N(\xi_{j,N})\,P_{N+1}(\xi_{j,N})}$	$\frac{1-\xi_{j,N}}{N^2\left(P_{N-1}(\xi_{j,N})\right)^2}$	$\frac{2}{N(N-1)\left(P_{N-1}(\xi_{j,N})\right)^2}$
Range	$j = 1, \ldots, N$	$j = 2, \ldots, N$	$j = 2, \ldots, N-1$
Error factor	$\psi_N^{(0)} = \frac{2^{2N+1}(N!)^4}{(2N+1)\left((2N)!\right)^3}$	$\psi_N^{(1)} = \frac{2^{2N-1}N\left((N-1)!\right)^4}{\left((2N-1)!\right)^3}$	$\psi_N^{(2)} = \frac{2^{2N-1}N(N-1)^3\left((N-2)!\right)^4}{(2N-1)\left((2N-2)!\right)^3}$
Asymptotic rate	$\widetilde{\psi}_N^{(0)} \sim \frac{\pi}{2^{2N}\,(2N+1)\,(2N-1)!}$	$\widetilde{\psi}_N^{(1)} \sim \frac{\pi}{2^{2N-1}\,(2N-1)!}$	$\widetilde{\psi}_N^{(2)} \sim \frac{(2N-1)\,\pi}{2^{2N-2}\,(2N-2)\,(2N-2)!}$
Bound on $\mathcal{Q}_N$	$\beta_N^{(0)} = \psi_N^{(0)}\,\mathbb{K}_{2N}$	$\beta_N^{(1)} = \psi_N^{(1)}\,\mathbb{K}_{2N-1}$	$\beta_N^{(2)} = \psi_N^{(2)}\,\mathbb{K}_{2N-2}$

Table 1: Quadrature results required for conducting and implementing the error analysis in §2.3. The presented Radau abscissae $\xi_{j,N}$, weights $w_{j,N}$ and bound on the quadrature error $\mathcal{Q}_N$ are for so-called left-Radau quadrature; those for right-Radau quadrature, in which the assigned node is $\widetilde{\xi}_{N,N} = 1$, satisfy $\widetilde{\xi}_{j,N} = -\xi_{N+1-j,N}$, $\widetilde{w}_{j,N} = w_{N+1-j,N}$ and $\mathcal{Q}_N = \widetilde{\mathcal{Q}}_N$. The theoretical bounds $\beta_N^{(\nu)}$ (which utilise (7)) on $\mathcal{Q}_N$ are validated on a test problem in Figure 1.

Problem	name	solution $y(x)$	kernel $K(x,\xi)$	λ
1	smooth	$\sin x + 3x^4$	$x\xi^3 + x^2\xi + 4$	$\frac{1}{10}$
2	Runge	$\frac{1}{1+25x^2}$	$(x+\xi)(5x-2\xi)$	$\frac{1}{5}$
3	steep	e^{-12x}	$2x^3 + 4x^2\xi + \xi^2$	$\frac{1}{2}$
4	oscillatory	$\cos 15x$	$\cos x + \sin 2\xi$	$\frac{1}{3}$

Table 2: Test problems with solutions of four qualitatively distinct forms. The Runge phenomenon [24, 25], extreme gradient and high-frequency oscillations, in the solutions of problems 2, 3 and 4 respectively, offer well-documented challenges to approximation methods.

Trial function	$v = 1$		$v = g$		$v = y$	
Norm type	External	Internal	External	Internal	External	Internal
Problem 1	8.000	8.000	0.526	1.869	1.499	1.748
Problem 2	8.667	8.667	1.408	2.967	2.631	2.631
Problem 3	4.667	5.105	0.387	0.470	0.324	0.324
Problem 4	2.000	2.000	3.882×10^{-2}	1.270	8.761×10^{-2}	1.247

Table 3: Comparison of the error-factor component $\|\mathcal{K}\,v\| \,/\, \|v\|$ computed using (32) and (33), respectively the external- and internal-modulus norm formulae. Comparisons are for three trial functions, the "standard" $v = 1$, the source function $v = g$ and the exact solution $v = y$. For all problems, $\|\mathcal{K}\,v\| \,/\, \|v\|$ is maximised using the trial function $v = 1$, which is accordingly used in the subsequent computation of error-bound suprema. For this norm, the "outlier", in terms of magnitude, is the highly oscillatory solution of Problem 4.

	$N = 10$			$N = 20$			$N = 30$		
Trial function	$u = 1$	$u = g$	$u = y_N$	$u = 1$	$u = g$	$u = y_N$	$u = 1$	$u = g$	$u = y_N$
Problem 1	5.000	1.176	2.949	5.000	1.176	3.166	5.000	1.176	3.211
Problem 2	3.144	0.9812	0.9929	3.144	0.9774	0.9788	3.144	0.9773	0.9787
Problem 3	457.5	0.8328	335.2	457.5	0.8328	422.2	457.5	0.8328	441.7
Problem 4	2.518	0.9916	1.678	2.518	0.9725	2.023	2.518	0.9725	2.082

Table 4: Comparison of the error-factor component $\|U_N\| \,/\, \|u\|$, equivalently $\left\|(\mathcal{I} - \lambda\,\mathcal{K}_N)^{-1}u\right\| \,/\, \|u\|$, computed using (26). Comparisons are for three trial functions $u = 1$, $u = g$ and the numerical solution $u = y_N$. For all problems, $\|U_N\| \,/\, \|u\|$ is maximised using the trial function $u = 1$, which is accordingly used in the subsequent computation of error-bound suprema. For this norm, the "outlier", in terms of magnitude, is the steep solution of Problem 3.

$\mathcal{B}_N/\mathcal{E}_N$	$N = 10$	$N = 20$	$N = 30$
Problem 1	4.190	4.162	4.157
Problem 2	4.251	4.251	4.251
Problem 3	14.18	4.162	3.382
Problem 4	1.176	1.176	1.176

Table 5: Values of the ratio $\mathcal{B}_N/\mathcal{E}_N$ (predicted error bound to actual error in numerical solution) for $\nu = 0$ using trial functions $u = v = 1$ in the four test problems. The external bound (32) was used in the computation of $\|\mathcal{K}\,v\|$ in (29). Results for $\nu = 1, 2$ are qualitatively similar. In all cases, the ratio converges with increasing N, always exceed unity, and are strictly of order $\mathcal{O}(1)$. The predicted bounds are best, in a relative sense, for Problem 4, despite the highly oscillatory nature of its solution.

	$N = 10$	$N = 20$	$N = 30$
Problem 1	8.124×10^{-22}	2.038×10^{-56}	6.641×10^{-96}
Problem 2	1.929×10^{-2}	3.691×10^{-4}	6.946×10^{-6}
Problem 3	6.838×10^{-2}	7.006×10^{-16}	4.168×10^{-34}
Problem 4	8.802×10^{-3}	3.272×10^{-14}	1.596×10^{-30}

Table 6: Computed values of $\|y_N - \lambda\,\mathcal{K}\,y_N - g\|$ for $\nu = 0$ used in estimating $\mathcal{B}_N$ via (16). This component of the predicted error is immutable, being unaffected by any of the approximations made in §2.4. Results for $\nu = 1, 2$ are qualitatively similar.

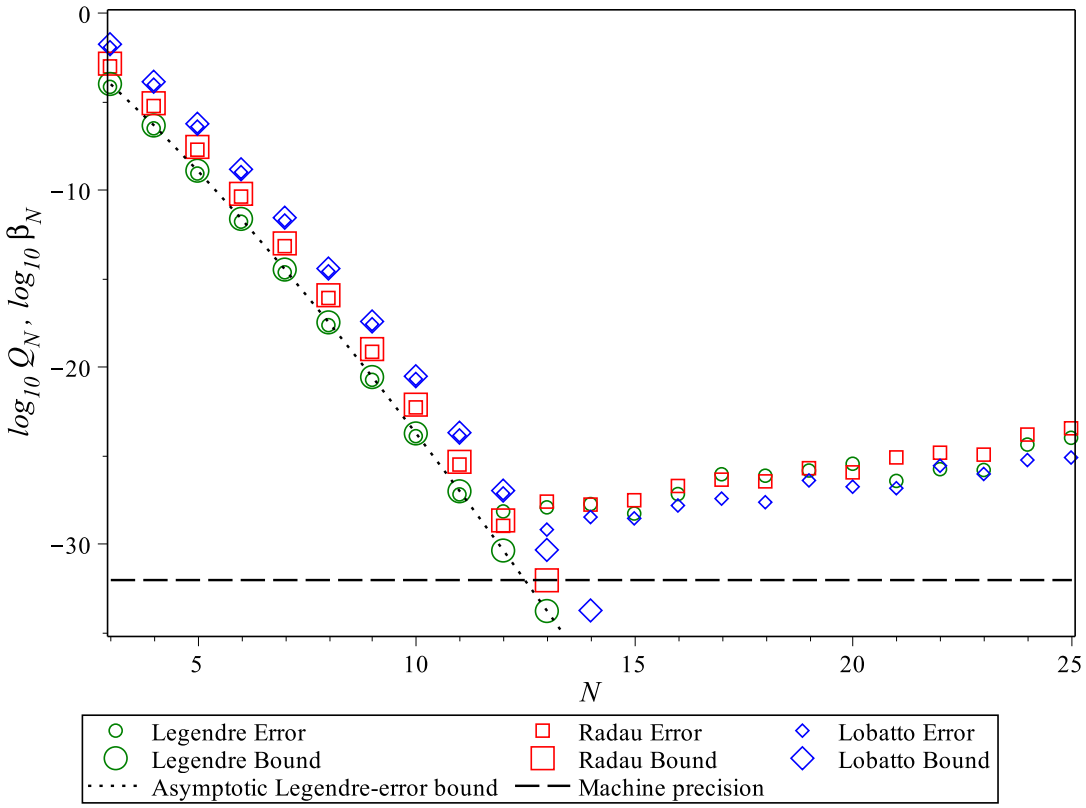

Figure 1: Logarithmic plot showing the close agreement between the predicted error bounds $\beta_N^{(0,1,2)}$ on $\mathcal{Q}_N$ (large symbols) in the last row of Table 1, the asymptotic Legendre-error bound (8) for $\widetilde{\beta}_N^{(0)}$ (dotted line) and the actual computational errors $\mathcal{Q}_N$ (small symbols). For illustrative purposes, the functions $K(x,\xi) = 1$ and $u(\xi) = \cos\xi + \sin\xi$ have been chosen in (7), and hence the excellent agreement is due to the infinite differentiability of the test function $u(\xi)$. All calculations were performed in the algebraic manipulator `Maple` in an enforced machine precision of 10^{-32} (dashed line), slightly above which the computational error exhibits the typical positive-gradient round-off plateau for increasing N. The predictions $\psi_N^{(1)}/\psi_N^{(0)} = 4N+2$ and $\psi_N^{(2)}/\psi_N^{(1)} = 4N+\frac{1}{N-1}$ (obtained from Table 1) are evident: before reaching the round-off plateau, the accuracy of the quadrature rule is eroded by each addition of an assigned abscissa.

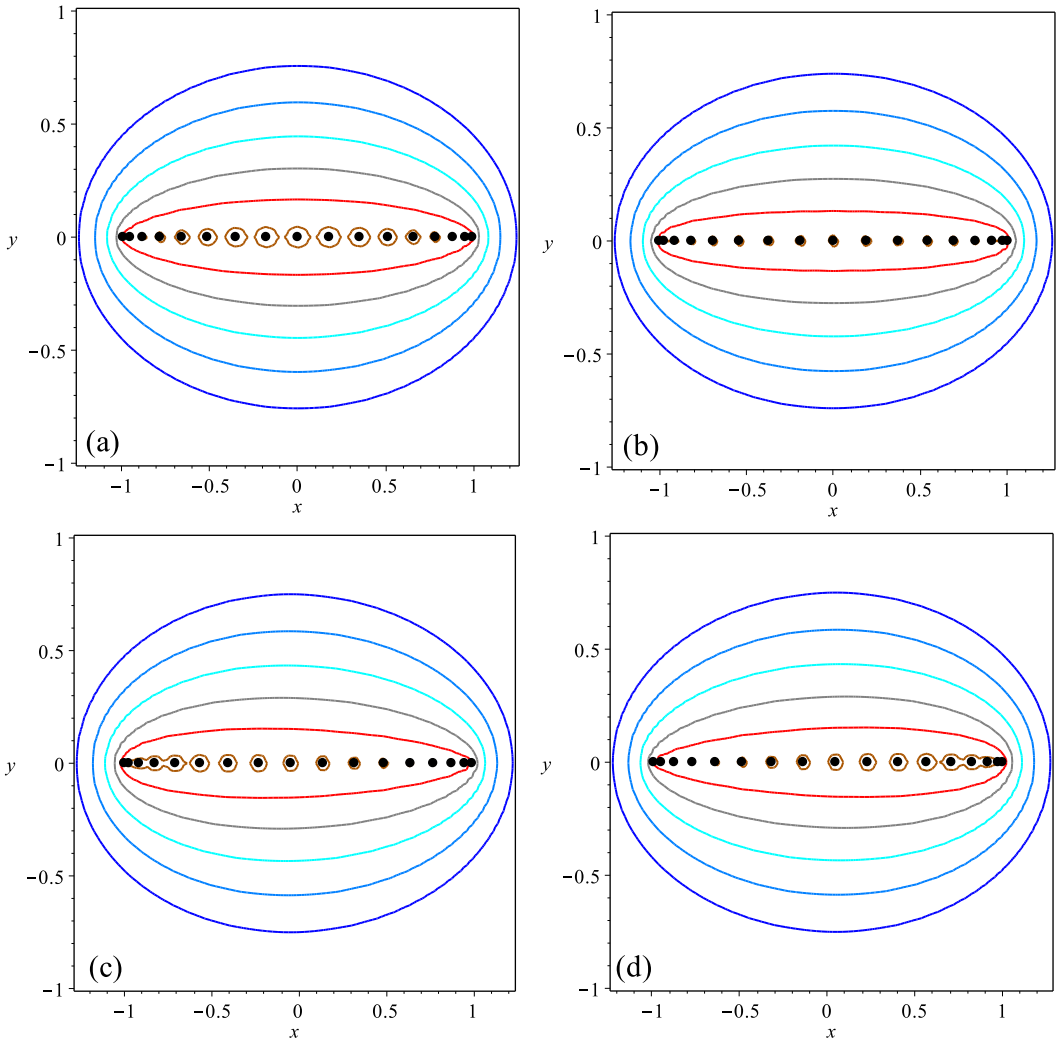

Figure 2: Complex contour plots (*cf.* [26, 22]) of the monic-polynomial equipotentials $|p_N(x+iy)| = 10^{-m}$ with roots at the (a) Legendre, (b) Lobatto, (c) left-Radau and (d) right-Radau nodes $\xi_{j,N}$. Here $N = 17$ and $m = 0(1)5$, with $m = 0$ and $m = 5$ respectively corresponding to the largest and smallest (adjacent to the nodes) contours. It is the flattish "cigar-like" profiles of the contours in the neighbourhood of $x \in [-1, 1]$ that give rise [26, Ch.5] to the spectral convergence observed in Figure 1 when using the abscissae summarised in Table 1.

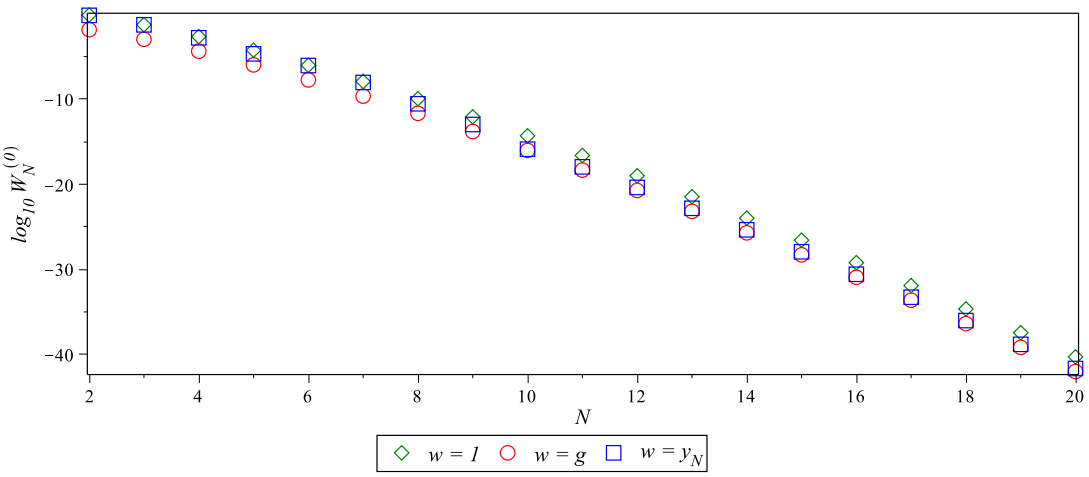

Figure 3: Logarithmic plot of $\mathcal{W}_N^{(0)}$ for Problem 4 and $w = 1$, $w = g$ and $w = y_N$ on the Legendre nodes. In the interests of clarity, the qualitatively identical and quantitatively similar results for Radau and Lobatto nodes are omitted. By (21) and (22), note that $\mathcal{W}_N^{(0)}$ is explicitly dependent upon only N and $\mathcal{K}$, the dependence on $\mathcal{K}_N$ being implicit via the quadrature abscissae and weights.

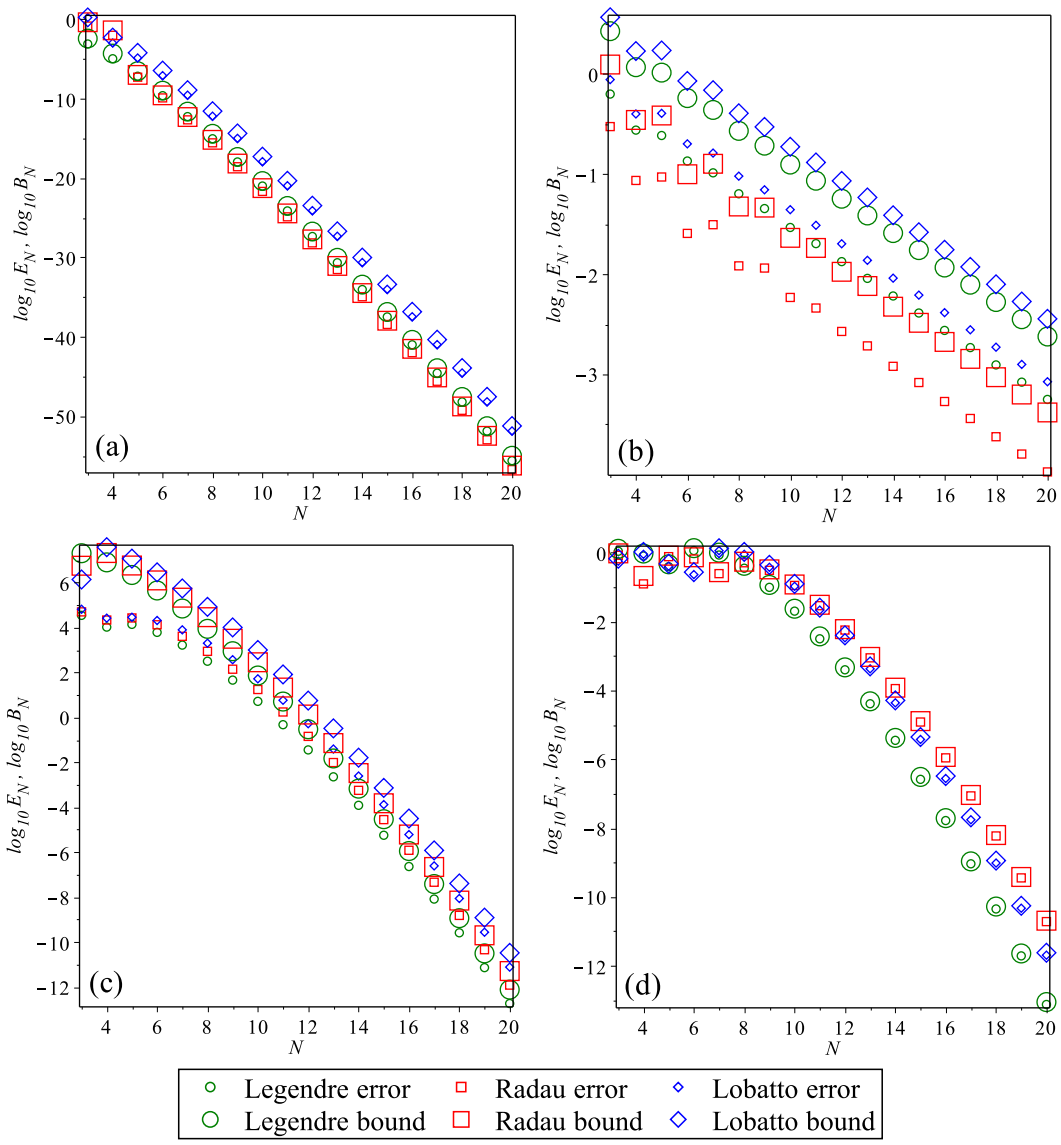

Figure 4: Logarithmic plots comparing theoretically predicted error bounds $\mathcal{B}_N$ (large symbols) and numerical computational errors $\mathcal{E}_N$ (corresponding small symbols) for Problems (a) 1 ("smooth"), (b) 2 ("Runge"), (c) 3 ("steep") and (d) 4 ("highly oscillatory"). Note the disparate vertical scales on each plot, the Runge problem displaying the slowest convergence with N; the "steep" and "oscillatory" errors are of comparable magnitude. Note that, for a given N, the magnitudes of the computed errors do not necessarily increase monotonically with ν for all test problems, as suggested by the isolated asymptotic rates in Table 1.

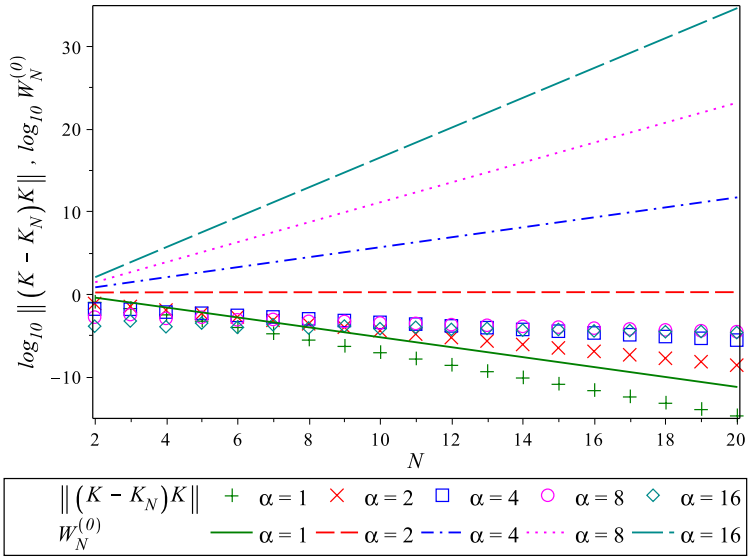

Figure 5: Logarithmic plot of $\|(\mathcal{K}-\mathcal{K}_N)\,\mathcal{K}\|$ computed using $w=1$ (symbols) and its theoretical bound $\mathcal{W}_N^{(0)}$ given by (37) (lines) for different values of α. Numerical results confirm spectral convergence of $\|(\mathcal{K}-\mathcal{K}_N)\,\mathcal{K}\|$ to zero with N, whereas exponential divergence of $\mathcal{W}_N^{(0)}$ is predicted for $\alpha > 2$. Note also the near-independence of this phenomenon on the value of $\alpha \gg 1$. The conclusion is that the theory of §2 remains valid for all α.

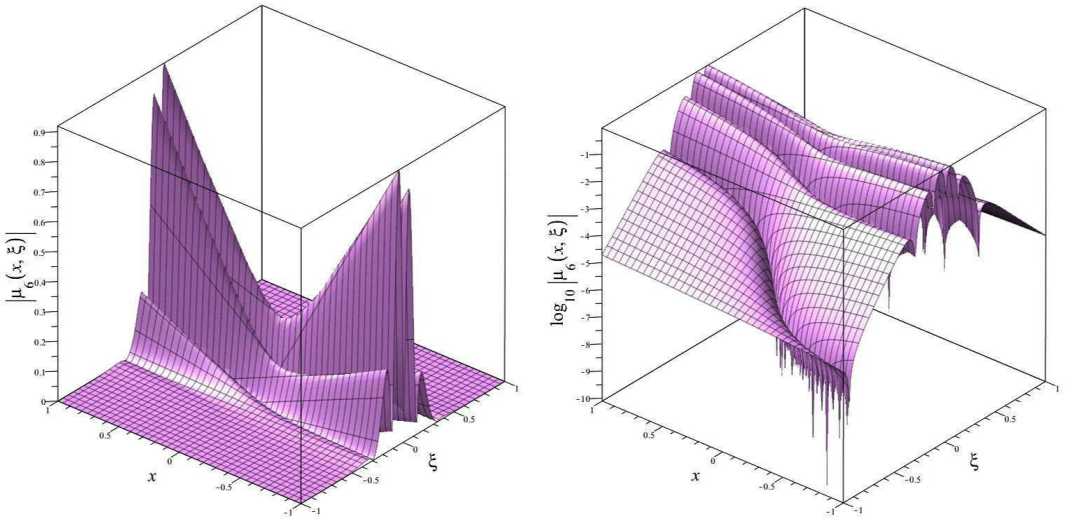

Figure 6: Plot (left) and logarithmic plot (right) of $|\mu_6(x,\xi)|$, with $\alpha=4$, showing both the highly localised suprema (independent of M) at $x=\pm1$ discussed after (35), and the near-global small magnitude discussed in the main body of the text.

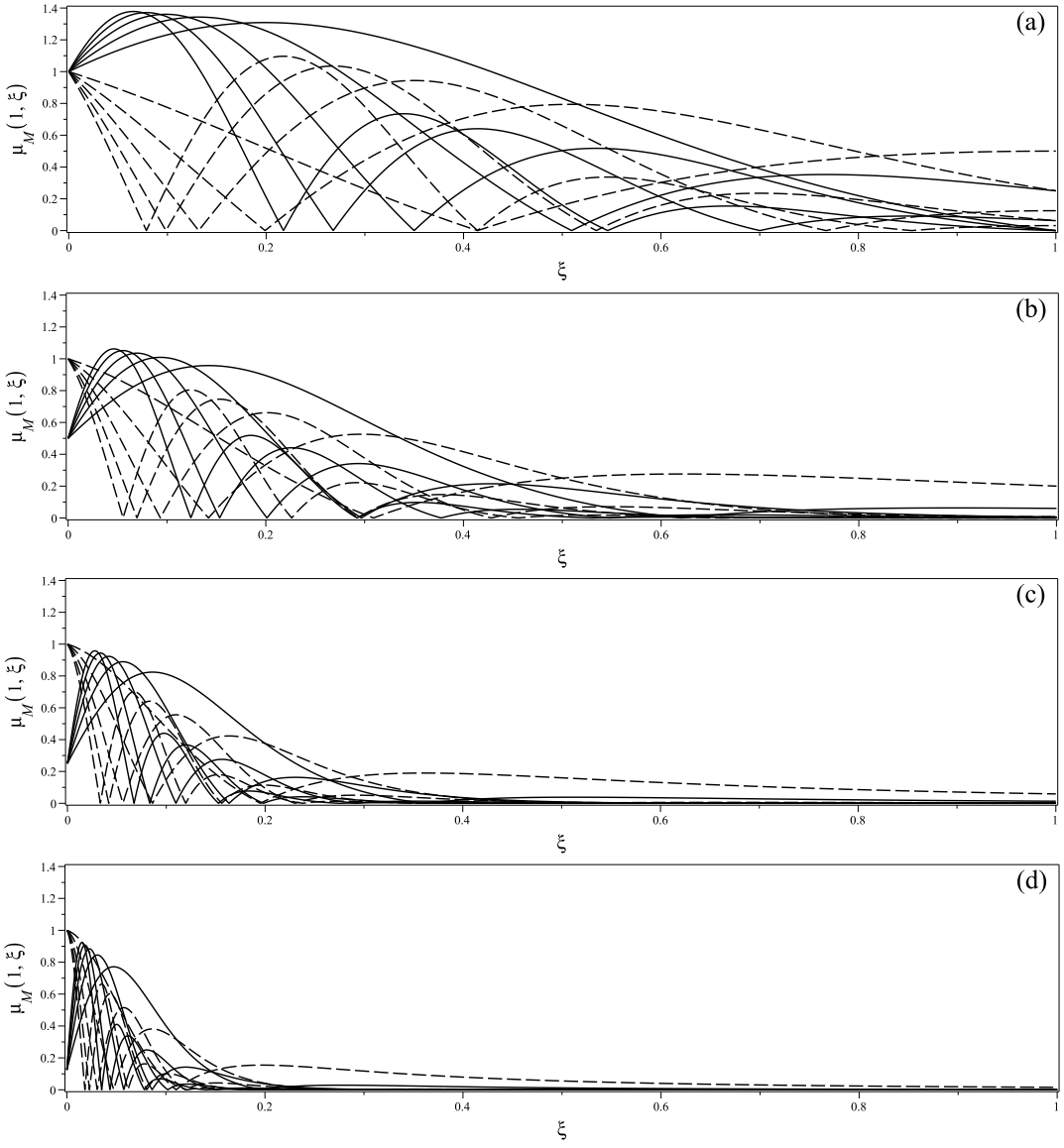

Figure 7: Plots in $\xi \in [0,1]$ of the normalised function $\mu_M(1,\xi)$ given by (36) for $M = 1$ to $M = 8$ and (a) $|\alpha| = 1$, (b) $|\alpha| = 2$, (c) $|\alpha| = 4$ and (d) $|\alpha| = 8$. Solid/dashed lines correspond to odd/even values of M, and local maxima away from $\xi = 0$ decrease with increasing M. Curves for $\xi \in [-1,0]$ are given by symmetry/antisymmetry for M even/odd. Clearly evident is the increasing localisation, discussed in the text, of the suprema with increasing $|\alpha|$.

***Response to Reviewers**

Click here to download Response to Reviewers: AMC-D-16-02821-response-to-reviewers.txt

Re paper AMC-D-16-02821-revised-version.
==========

The handful of minor cosmetic changes requested by reviewer #1 (these was only one review) has been fully implemented.